Lethaia
AN INTERNATIONAL JOURNAL OF PALAEONTOLOGY AND STRATIGRAPHY

Integrated magnetobiochronology of the Early/Middle Eocene transition at Agost (Spain): Implications for defining the Ypresian/Lutetian boundary stratotype

JUAN C. LARRASOAÑA, CONCEPCIÓN GONZALVO, EUSTOQUIO MOLINA, SIMONETTA MONECHI, SILVIA ORTIZ, FLAVIA TORI AND JOSEP TOSQUELLA

LETHAIA

Larrasoaña, J.C., Gonzalvo, C., Molina, E., Monechi, S., Ortiz, S., Tori, F. & Tosquella, J. 2008: Integrated magnetobiochronology of the Early/Middle Eocene transition at Agost (Spain): Implications for defining the Ypresian/Lutetian boundary stratotype. *Lethaia*, Vol. 41, pp. 395–415

In this paper, we present an integrated study of a 115-m-thick section that spans the Ypresian/Lutetian boundary at Agost (Betic Cordillera, SE Spain). Our study includes magnetostratigraphic results and biostratigraphic and palaeoenvironmental data derived from planktic foraminifera, small and larger benthic foraminifera, and calcareous nannofossils. Our results demonstrate that the Agost section is continuous and spans from Zones P9 to P12 (E7 to E10), Zones CP11 to CP14a (NP13 to NP16), Zones SBZ11 to SBZ15, and Chrons C22n to C19r. The first occurrence (FO) of *H. nuttalli* (base of P10) and the FO of *G. nuttalli* (base of E8) are found within Chron C20r, at a much younger age (3–5 Myr) than previously considered in standard calibration schemes. Similarly, the boundary between SBZ12 and SBZ13 is located within Chron C21n, also at a younger age than previously considered. On the contrary, the FO of *B. inflatus* (base of CP12b) is found within Chron C21r, which conforms to the magnetostratigraphically calibrated age of ca. 48 Ma (middle part of C21r) considered in standard calibration schemes. These results corroborate earlier studies and indicate that all the events that have been proposed to mark the Ypresian/Lutetian boundary appear at different stratigraphic intervals and have different ages. Based on our results from Agost and on data from other sections elsewhere, we suggest that the Ypresian/Lutetian boundary might be approximated by the FO of *B. inflatus* (base of CP12b). The Agost section might be considered as a potential candidate to locate the Global Stratotype Section and Point (GSSP) of the base of the Lutetian Stage, because it includes all the events that might be selected as marker events for the Ypresian/Lutetian boundary and it fulfils most of the geological, biostratigraphic and infrastructure requirements demanded for definition of a GSSP. □*Agost*, *Betic Cordillera*, *biostratigraphy*, *calcareous nannofossils*, *Global Stratotype Section and Point*, *larger benthic foraminifera*, *magnetostratigraphy*, *planktic foraminifera*, *small benthic foraminifera*, *Ypresian/Lutetian boundary*.

Juan C. Larrasoaña [jclarra@ija.csic.es], Institut de Ciències de la Terra Jaume Almera, CSIC, Solé Sabarís s/n, 08028 Barcelona, Spain; Concepción Gonzalvo [concha@unizar.es], Eustoquio Molina [emolina@unizar.es] and Silvia Ortiz [silortiz@unizar.es], Departamento de Ciencias de la Tierra, Universidad de Zaragoza, Pedro Cerbuna 12, 50009 Zaragoza, Spain; Simonetta Monechi [monechi@unifi.it] and Flavia Tori [flavia.tori@unifi.it], Dipartimento di Scienze della Terra, Università di Firenze, via La Pira 4, 50121 Firenze, Italy; Josep Tosquella [josep@uhu.es], Departamento de Geodinámica y Paleontología, Facultad de Ciencias Experimentales, Universidad de Huelva, Avenida de las Fuerzas Armadas s/n, 21071 Huelva, Spain; *manuscript received on 16/05/07; and manuscript accepted on 20/12/07.*

Definition of global reference points and selection of boundary stratotypes is important for delineating the chronostratigraphic scale that frames the geological history of the Earth (Gradstein *et al.* 2004). Still pending definition is the base of the Lutetian Stage (Early/Middle Eocene boundary). This boundary is currently marked by the FO (first occurrence) of *Hantkenina nuttalli* (base of P10 of Berggren *et al.* 1995) (see Luterbacher *et al.* 2004), and has classically been correlated to the top of Chron C22n on the basis of magnetostratigraphic results from Gubbio, Italy (Lowrie *et al.* 1982; Napoleone *et al.* 1983). However, a precise correlation of this event to the geomagnetic polarity timescale (GPTS) is still to be established, since identification of planktic foraminifera in the Italian sections is made difficult by the hard nature of the host sediments and by the poor preservation of planktic foraminifera in some levels (Lowrie *et al.* 1982; Napoleone *et al.* 1983; Opdyke & Channell 1995). Further complications arise from

DOI 10.1111/j.1502-3931.2008.00096.x

new results retrieved from drill cores in Tanzania (Pearson *et al.* 2004). These results suggest that the FO of *H. nuttalli* occurs at different stratigraphic intervals in different sections, and therefore cast doubt on the usefulness of this event as a reliable marker for the Ypresian/Lutetian boundary (Berggren & Pearson 2005, 2006). Alternative markers of the boundary include the FO of the planktic foraminifera *Guembelitrioides nuttalli* (= *Globigerinoides higginsi*) (base of E8 of Berggren & Pearson 2005, 2006), the FO of calcareous nannofossil *Blackites inflatus* (base of CP12b of Okada & Bukry 1980), and the boundary between shallow benthic Zones SBZ12 and SBZ13 (Serra-Kiel *et al.* 1998). Unfortunately, assessing the suitability of these markers has been made difficult because many sections around the world either contain sedimentary hiatuses at the boundary (see reviews by Aubry 1995 and Opdyke & Channell 1995) or lack magnetostratigraphic or biostratigraphic results with the appropriate resolution or quality (Galbrun 1992; van Fossen 1997; Molina *et al.* 2000; Ogg & Bardot 2001; Pearson *et al.* 2004; Bowles 2006; Molina *et al.* 2006; Payros *et al.* 2006; Suganuma & Ogg 2006). A notable exception is the Gorrondatxe section, which has recently been studied by Bernaola *et al.* (2006) and Payros *et al.* (2007) in the Basque–Cantabrian basin (Spain). This section provides a new magnetobiostratigraphic correlation scheme that bears important implications for defining the Ypresian/Lutetian boundary. All possible markers of the Ypresian/Lutetian boundary appear in the section, although at different stratigraphic levels. The FOs of *H. nuttalli* and *G. nuttalli* occur at about 43.5 Ma and 45.5 Ma, respectively (Payros *et al.* 2007). These ages are about 3 to 5 Myr younger compared to classic sections from Gubbio (Lowrie *et al.* 1982; Napoleone *et al.* 1983), where standard calibration schemes of planktic foraminifera are based on (Berggren *et al.* 1995; Luterbacher *et al.* 2004; Berggren & Pearson 2005, 2006; Pearson *et al.* 2006a). In view of the implications of the results of Bernaola *et al.* (2006) and Payros *et al.* (2007), and to shed light on the calibration of the Ypresian/Lutetian boundary, new sections need to be studied and examined.

In this paper, we present an integrated study of a 115-m-thick section that spans the Ypresian/Lutetian boundary at Agost (Spain). This section is located in the vicinity of the section studied previously by Molina *et al.* (2000), but offers better outcrop and fossil preservation conditions. Our new study includes magnetostratigraphic results and biostratigraphic and palaeoenvironmental data derived from planktic foraminifera, small and larger benthic foraminifera, and calcareous nannofossils. Our results provide a magnetobiostratigraphic calibration which is largely consistent with that proposed in the Gorrondatxe section, and therefore reinforce the suggestion by Payros *et al.* (2007) to reconsider standard calibration schemes for the Ypresian/Lutetian boundary (Berggren *et al.* 1995; Luterbacher *et al.* 2004; Berggren & Pearson 2005, 2006; Pearson *et al.* 2006a). In that case, the Agost section presented here may be considered as a suitable candidate for defining the Early/Middle Eocene boundary stratotype.

Geological setting

The Agost section is located ca. 1 km to the north of the village of Agost (Alicante, southeast Spain), in the so-called Lomas de la Beata area (Fig. 1). During the Eocene, the studied area belonged to the passive margin of Iberia. Carbonate sedimentation in the platform gave way to pelagic sediments, turbidites

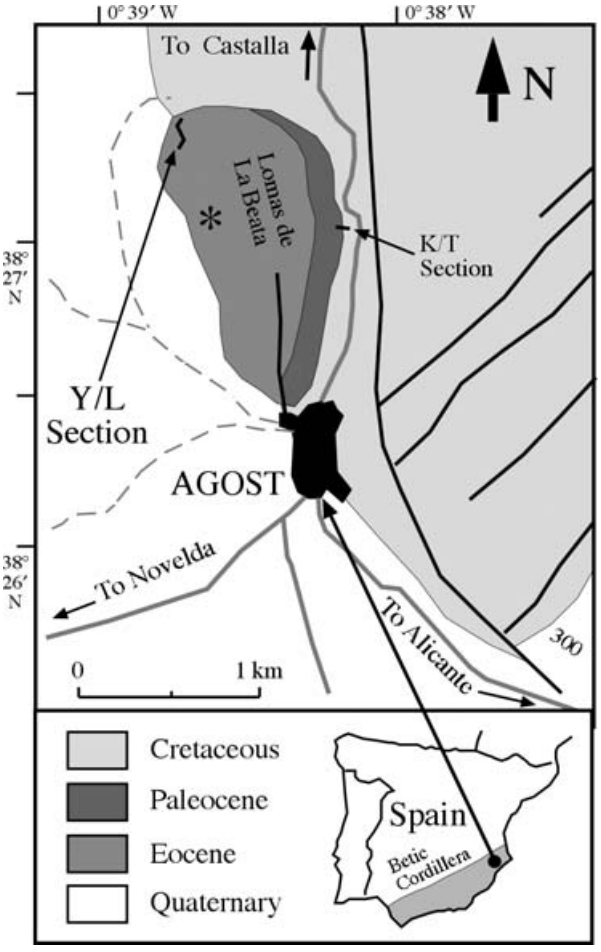

Fig. 1. Location of the Agost section presented in this study. The asterisk indicates the location of the Ypresian/Lutetian section studied previously by Molina *et al.* (2000). The location of the K/T boundary section (Groot *et al.* 1989) is also shown.

and mass flow deposits in the continental slope located southwards (Geel 2000; Alonso-Zarza *et al.* 2002). These sediments were folded and uplifted during the Miocene collision that led to formation of the Betic Cordillera in southern Spain (Guerrera *et al.* 2006). Nowadays, these sediments are exposed at the Agost section striking broadly north to south and displaying a gentle westward dipping of about 15–20° (Molina *et al.* 2000). The section is composed of 115 m of marls with intercalated limestone and sandstone beds (Fig. 2). Marls have a distinctive greenish-greyish colour and commonly constitute several-metre-thick intervals. Limestones range between white and light grey in colour, and are often less than 50 cm thick. Marls and limestones correspond to hemipelagic sediments, and predominate in the lower and upper parts of the section. Sandstones have beige or yellow colours, and range between few centimetres and 2 m thick. Some sandstone beds show evidence of slumping and, in some cases, contain embedded limestone boulders. Sandstones correspond to resedimented slope deposits (turbidites and mass flows) accumulated in the outer part of carbonate platforms (Geel 2000; Alonso-Zarza *et al.* 2002). Sandstone beds are clustered in several thick packages that constitute a characteristic stratigraphic interval located in the middle upper part of the section. The Agost section is affected by two small faults that show minor displacements of less than 3–4 m and, therefore, do not disrupt the stratigraphic sequence.

Methods

The magnetostratigraphic study is based on 87 palaeomagnetic sites distributed along 115 m of sedimentary succession. Between one and two oriented cores were taken at 84 of these sites with a portable gas-powered drill. Sampling was focused, when possible, on hemipelagic mudstones and marly–limestones. In the middle part of the section, samples were also collected from sandstone layers in which no evidence for overturned beds or slumping was observed. This sampling scheme gives a mean resolution of 1.4 m, which allows identification of geomagnetic polarity reversals located near the Ypresian/Lutetian boundary according to preliminary correlation of biostratigraphic data (Molina *et al.* 2000) to the revised GPTS (Luterbacher *et al.* 2004). Three additional samples were taken in three limestone boulders embedded in turbidites. Palaeomagnetic analyses were made using a 2G superconducting rock magnetometer at the palaeomagnetic laboratory of the Institute of Earth Sciences *Jaume Almera* (CSIC-Universitat de Barcelona). The noise level of the magnetometer is less than 7×10^{-6} A/m, which is lower than the natural remanent magnetization (NRM) of the samples measured. Thermal demagnetization of at least one sample per site was done using a MMTD-80 furnace (Magnetic Measurements Ltd, Aughton, UK). Thermal treatment involved between eight and 14 steps at intervals of 150, 100, 50, 30 and 20°C to a maximum temperature of 600°C. Demagnetization of a set of pilot samples representative of all the lithologies allowed optimization of the demagnetization steps to allow accurate calculation of the characteristic remanent magnetization (ChRM) directions minimizing heating and formation of new magnetic phases in the oven. ChRM directions were calculated by fitting linear trends in orthogonal demagnetization plots using the principal component analysis method (Kirschvink 1980).

For the study of planktic and small benthic foraminifera, and of calcareous nannofossils, 86 samples, most of them in marls, were collected throughout the section. Each of these samples was divided into two parts. The first part was disaggregated in water and washed through a 100-μm sieve. Each sample was cleaned using ultrasonic agitation, and subsequent washing and sieving were repeated until a clean foraminiferal residue was obtained. This residue was dried in an oven at a temperature of 50°C. Quantitative analyses of planktic foraminifera from 86 samples were based on representative random splits (using an Otto microsplitter) of more than 300 specimens. The rest of each foraminiferal residue was examined for identification of rare species. Planktic foraminiferal biozones have been established using the scheme proposed for the Betic Cordilleras by Gonzalvo & Molina (1998), the standard tropical–subtropical zonation scheme of Berggren *et al.* (1995) and its latest revised versions (Berggren & Pearson 2005, 2006). A detailed review of the distribution of relevant species is given in Pearson *et al.* (2006a, b). Small benthic foraminifera have been studied in 30 samples in order to examine their potential biostratigraphic value across the Ypresian/Lutetian boundary (Berggren & Miller 1989) and also to detect environmental changes (Thomas 2003) potentially associated to the boundary. The study was carried out by picking about 300 specimens from the same foraminiferal residue from which planktic foraminifera were analysed.

The raw material from the second part of each sample was used to prepare smear slides and study calcareous nannofossils. Smear slides of 61 samples were prepared weighing 0.05 g of sediment and mixing it with 15 mL of distilled water. Ten to twelve drops of the mixture were then spread on a

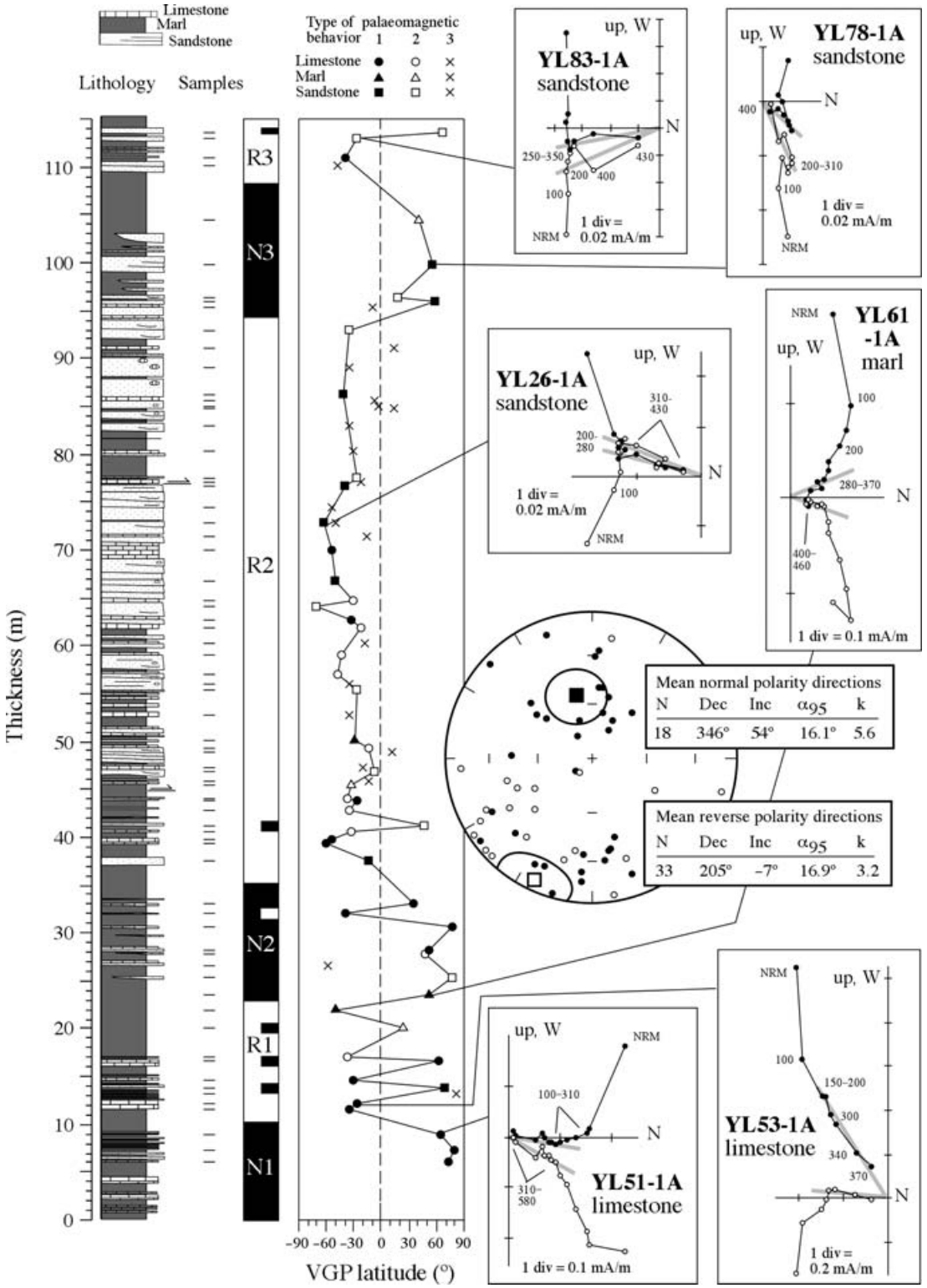

Fig. 2. Stratigraphic log and palaeomagnetic results from the Agost section. The position of the studied samples is plotted against the stratigraphic log of the section. Filled and open symbols indicate type 1 and type 2 samples, respectively, whereas crosses indicate type 3 samples. Circles, squares and triangles represent limestones, sandstones and marls, respectively. Examples of ortogonal demagnetization diagrams representative of different types of palaeomagnetic behaviour are shown after tilt correction. Grey lines indicate the best fit of the calculated ChRM directions. Reliable type 1 and type 2 ChRM directions are plotted after tilt correction in an equal-area stereonet (filled and open symbols represent projection in the lower and upper hemispheres, respectively), together with the mean direction and statistics of normal and reverse polarity directions.

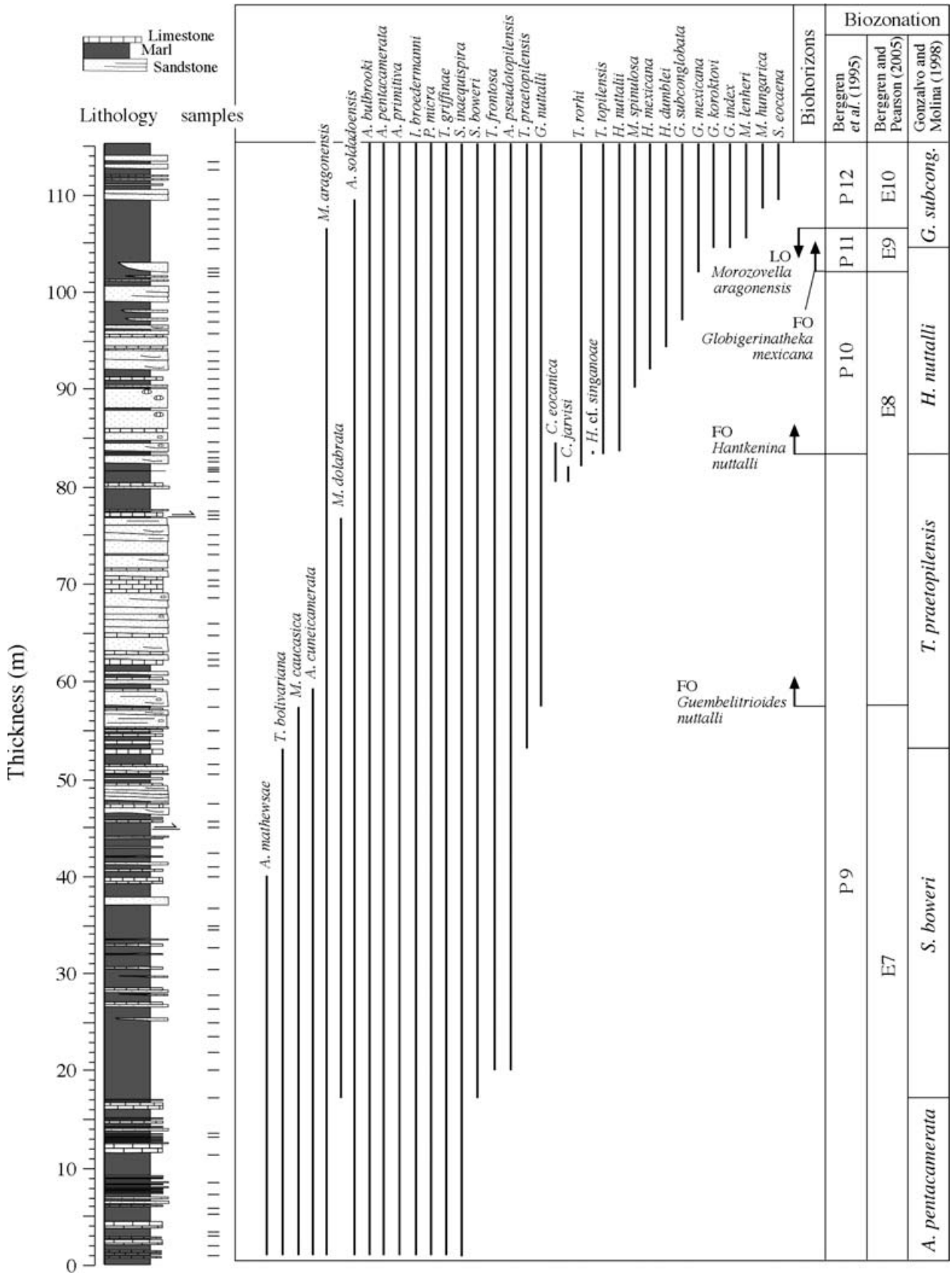

Fig. 3. Stratigraphic distribution of relevant planktic foraminifera and biozonation of the Agost section. The position of the studied samples is plotted against the stratigraphic log of the section.

glass cover slip and dried. In order to obtain the original nannofossil composition on the slide, neither ultrasonic cleaning nor centrifuge concentration was used. The slides were glued to the glass cover slips by means of a drop of Norland Optical Adhesive (NOA-65). Qualitative and semiquantitative analyses were performed by scanning two traverses of each smear slide in order to also detect rare species. Standard light microscope techniques were used at ×1260 magnification on a Zeiss Axioplan 2 Imaging (Carl Zeiss, Gottingen, Germany). Details and smallest forms were studied at a magnification of ×1890 or ×2000 when needed. Zonation of calcareous nannofossils is based on Martini (1971) and Okada & Bukry (1980).

Assemblages of larger benthic foraminifera were studied in eight samples collected at marly levels. Samples were washed in the laboratory, and individual specimens were separated and studied according to the following method. First, a binocular microscope was used to separate different morphotypes according to their diameter, shape and arrangement of septal filaments and granules. Then, individual specimens were split along the equatorial section to study inner features such as number of whorls, rate of opening of the spire (whorl radius), number of chambers, and septal and chamber shape. Embryo morphologies and proloculus diameter in megalospheric forms (A-forms) were also examined. Biostratigraphic range of nummulitid species was assigned following SBZ zones of Serra-Kiel *et al.* (1998).

Results

Magnetic stratigraphy

The natural remanent magnetization (NRM) of most of the studied samples is weak, usually between 500 and 2000×10^{-6} A/m. In most of the studied samples, a low temperature magnetization is unblocked below 300°C after removal of a viscous component at < 150°C (Fig. 2). This low temperature component is parallel to the present-day geomagnetic field in *in situ* coordinates and therefore lacks any geological significance for this study. Above 300°C, a ChRM can be identified in about 86% of the samples despite their overall weak intensities. The ChRM always unblocks below 580°C regardless of palaeomagnetic behaviour and lithology, indicating that magnetite (of probable detrital origin) is the main magnetic carrier. Three types of ChRM directions have been considered. Type 1 directions, which represent about 33% of the studied samples, show mostly linear trends directed to the origin of the orthogonal demagnetization plots. These directions have low to moderate errors and enable reliable polarity determinations. Type 2 directions (27% of the studied samples) show either less well-developed linear trends or incomplete demagnetizations due to the growing of new minerals during thermal treatment. These directions have errors larger than type 1 samples, but provide reliable polarity determinations by fitting clustered directions to the origin of the demagnetization plots. Type 3 directions (26% of the studied samples) have highly scattered directions derived from endpoints observed after removal of the low temperature component at > 300°C. These directions are associated to very weak magnetizations, and provide somehow ambiguous polarity determinations. Regardless of palaeomagnetic behaviour and lithology, the ChRM records both normal and reverse polarities after untilting the beds. It should be noted, however, that ChRM directions, especially those with reverse polarity, are highly scattered (Fig. 2). Moreover, the means of normal and reverse polarity directions are not antipodal. This behaviour is attributed to: (i) the overall weak intensity of most ChRM directions, which affects samples with both normal and reverse polarities; and (ii) the strong overlap of reverse polarity ChRM directions with the low-temperature component. Such a strong overlap has been previously reported by Groot *et al.* (1989) from Cretaceous and Palaeogene rocks collected along the K/T boundary in a section located just < 1 km southwest of the section studied here.

Since all the rocks sampled have similar striking and dip directions, the fold test cannot be applied in order to assess the origin of the ChRM. Application of the conglomerate test has neither been possible due to very weak magnetizations of the three samples collected in limestone boulders embedded in turbidite levels. Moreover, the high scattering of the ChRM directions provides non-significant results in the reversal test. Despite the lack of field tests constraining the origin of the ChRM, it is thought to represent a magnetization acquired at or near deposition because: (i) the sequence of polarity changes is independent of lithology and palaeomagnetic behaviour, and is rather consistent with biostratigraphic results; and (ii) previous palaeomagnetic results from the K/T boundary provide evidence for the absence of remagnetizations in Palaeogene rocks in the area (Groot *et al.* 1989).

Virtual geomagnetic pole (VGP) latitudes have been calculated using only reliable (type 1 and 2 samples) ChRM directions after untilting the beds back to their original horizontal position. Due to the scattering of the ChRM directions, the VGP latitudes calculated are often far from the expected value of

80–90°. Despite this, VGP latitudes indicative of normal and reverse polarity directions are not distributed randomly throughout the section, in such a way that an overall clear sequence of polarity reversals can be identified (Fig. 2). The most conspicuous pattern is a thick reverse polarity interval that spans the middle part of the section (labelled R2). Above R2, the top of the section is characterized by a short normal polarity interval (N3) that is overlain by a reverse polarity interval (R3). The lowermost part of the section is characterized by two short normal polarity intervals (N1 and N2). N1 and N2 are separated by an interval with alternating normal and reverse polarity samples, albeit the later being predominant. This interval might be interpreted as a reverse polarity interval (labelled R1) in which reverse polarity ChRM directions are particularly affected by the strong overprint with the low-temperature component.

Planktic foraminifera

Most samples contain assemblages of planktic foraminifera that are well preserved and represent more than 80% of the total foraminiferal content. Some samples contain high numbers of reworked planktic species, but this does not impede accurate biostratigraphic assignation of the studied samples. The planktic foraminiferal biostratigraphy of the Agost section is based on the first and last occurrences of significant species (Figs 3, 4), and allows us to identify the following subzones described by Gonzalvo & Molina (1998) for the Betic Cordillera: the upper part of the *Acarinina pentacamerata*, the *Subbotina boweri* and *Truncorotaloides praetopilensis* subzones classically attributed to the late Ypresian, and the *H. nuttalli* and *Globigerapsis subconglobata* subzones of the early Lutetian. In terms of standard planktic foraminiferal biozonation schemes, the absence of *Astrorotalia* (= *Planorotalites*) *palmerae* in the Agost section prevents identification of the base of Zone P9 of Berggren *et al.* (1995). Nevertheless, faunas from the lowermost part of the section include *A. pentacamerata*, *A. bullbrooki*, *A. soldadoensis*, *S. inaequispira*, *T. frontosa*, *Morozovella caucasica* and *M. aragonensis*, which are typical of Zone P9/E7. The FO of *G. nuttalli*, and hence the base of Zone E8 of Berggren & Pearson (2005, 2006), occurs at metre 57 within the lower part of R2. The occurrence of *Hantkenina* cf. *singanoae* at metre 83.6, and its gradual transition to *H. nuttalli* at the same interval, allows identification of the base of P10 of Berggren *et al.* (1995) in the upper part of R2. These results indicate that the interval at which hantkeninids appear is continuous. Noticeably, the occurrence of *Clavigerinella eocaenica* and *C. jarvisi* just before the appearance of hantkeninids might provide evidence for an excursion of tropical species due to an increase in seawater temperature. The absence of *G. kugleri* prevents identification of P11/E9. In the absence of this marker, the base of P11/E9 can be located at the FO of *G. mexicana* (Pearson *et al.* 2006b), which is found at metre 102 (within N3). Higher up in the section, the last occurrence (LO) of *M. aragonensis* marks the base of P12/E10 at metre 107, in the uppermost part of N3.

Calcareous nannofossils

The nannofossil assemblages are generally rich (37 to 85 taxa) and consist of well-diversified mid-latitude associations. Preservation of calcareous nannofossils varies from good/moderate to poor because of overgrowth and/or etching. Overall, preservation is better in the lower part of the section and in the marl levels. Reworked forms, mainly from the Cretaceous and sometimes from the Palaeocene, have been observed throughout the section with variable abundances. Few samples contain rare autochthonous nannofossil taxa together with very abundant microcarb, siliciclastic material, and/or reworked specimens, making biostratigraphic identification difficult. Calcareous nannofossil assemblages include mainly *Reticulofenestra dictyoda*, *R. scrippsae*, *R. hesslandii*, *R. bisecta* < 10 μm, *Sphenolithus moriformis* and *Coccolithus pelagicus.* In addition, Early/Middle Eocene species *Campylosphaera dela*, *Chiasmolithus solitus*, *Clausicoccus obrutus*, *Coronocyclus bramlettei*, *Discoaster barbadiensis*, *Ericsonia formosa*, *Sphenolithus radians*, *Zyghrablithus bijugatus*, and *Prinsiacee* < 3 μm, appear continuously throughout the section.

All the marker events of the Okada & Bukry (1980) and Martini (1971) zonations have been found from CP11 to CP14a and from NP13 to NP16, respectively (Figs 5, 6). The marker species used by Okada & Bukry (1980) give better resolution and show a more continuous occurrence in the section. The lowest 2 m of the section contain common *Coccolithus crassus*, abundant reticulofenestrid, only very small *Toweius* and no *Discoaster sublodoensis*, and can therefore be related to the upper part of CP11. The FRO (First Rare Occurrence) of *D. sublodoensis*, and hence the base of CP12a, is located at metre 3 within N1. This taxon shows continuous distribution from metre 13.2 upwards. The FO of *Blackites inflatus*, and therefore the base of CP12b, is found at metre 13.2 in the lower part of R1. Due to the scarce and/or discontinuous occurrence of *D. sublodoensis* and *B. inflatus* in the lower and upper part of their ranges, identification of the base of

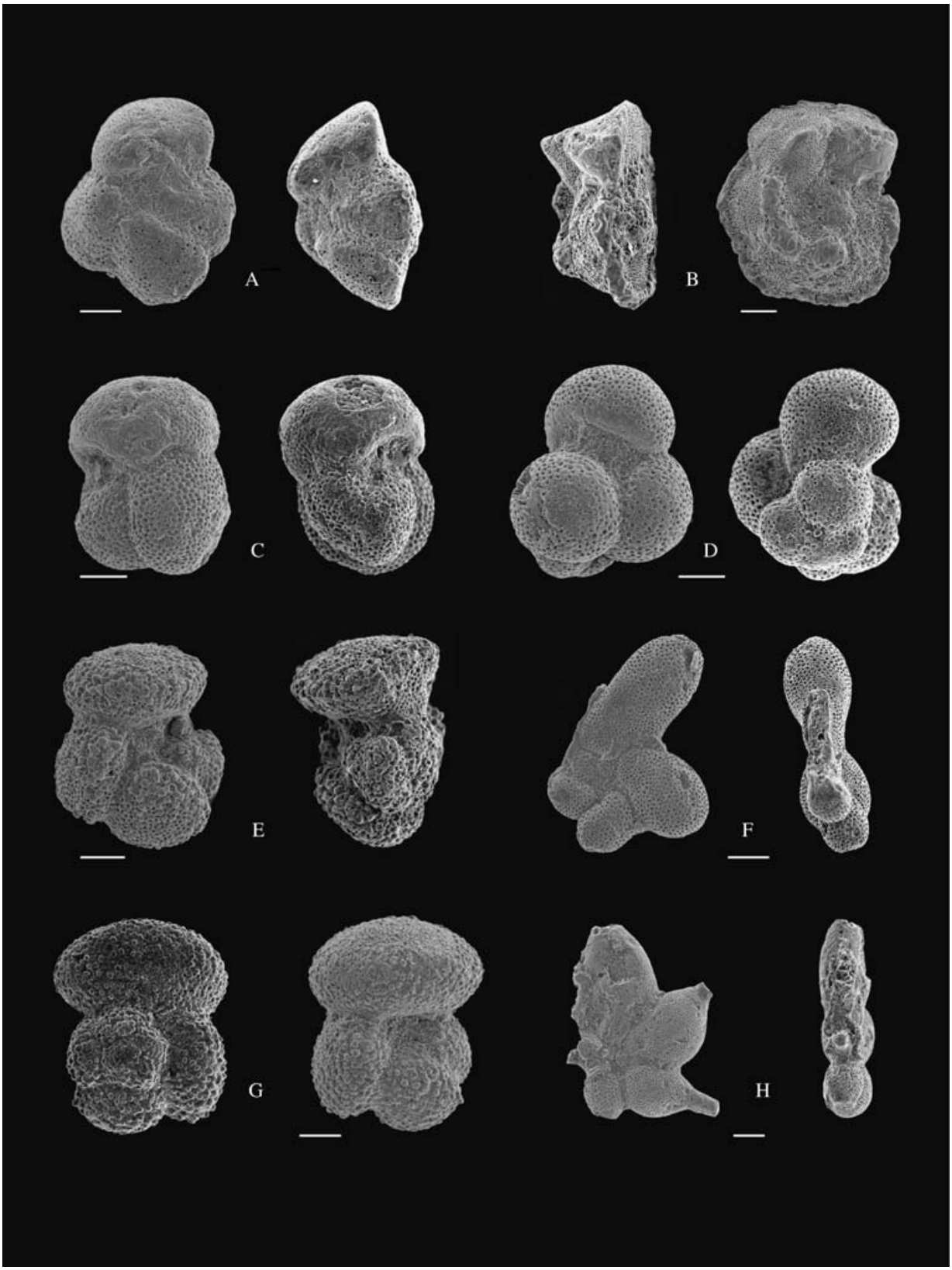

Fig. 4. Scanning electron microscope images of selected planktic foraminifera from the Agost section. □A. *Morozovella spinulosa* (metre 90.2); □B. *Morozovella caucasica* (metre 77); □C. *Turborotalia frontosa* (metre 104.5); □D. *Guembelitriodes nuttalli* (metre 90.2); □E. *Truncorotaloides rohri* (metre 104.5); □F. *Clavigerinella jarvisi* (metre 82); □G. *Truncorotaloides topilensis* (metre 104.5); □H. *Hantkenina mexicana* (metre 94.3). Scale bars = 100 μm.

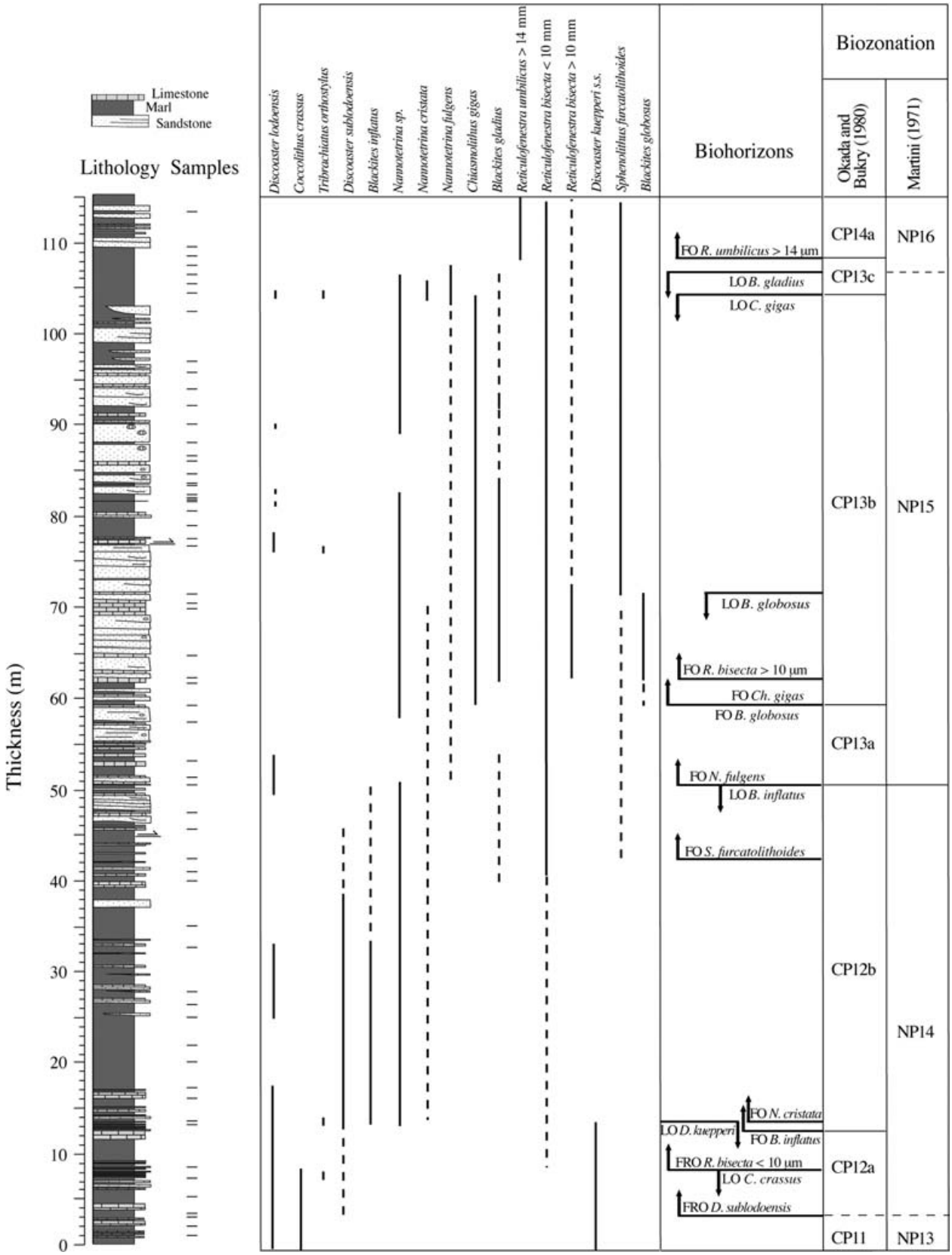

Fig. 5. Stratigraphic distribution of relevant calcareous nannofossils and biozonation of the Agost section. Dashed lines indicate discontinuous occurrences. The position of the studied samples is plotted against the stratigraphic log of the section.

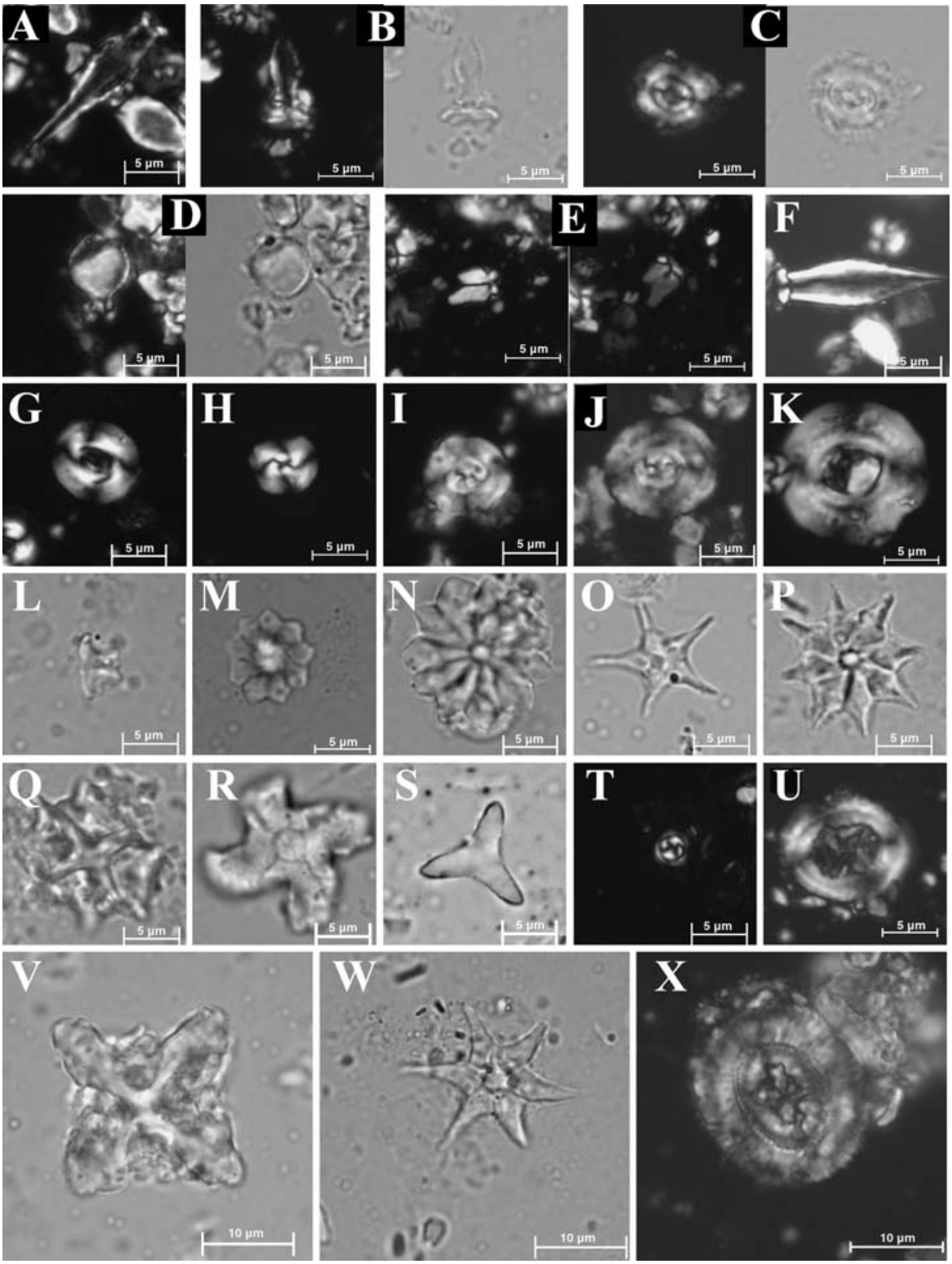

Fig. 6. Light microscope images of selected calcareous nannofossils from the Agost section. □A. *Blackites inflatus* (metre 13.2); □B. *B. gladius* (metre 81.7); □C. *Coccolithus crassus* (metre 3); □D. *Blackites globosus* (metre 62.3); □E. *Sphenolithus furcatholithoides* (metre 106.5); □F. *B. inflatus* (metre 45.7); □G. *Reticulofenestra dictyoda* (metre 45.7); □H. *R. scrippsae* (metre 2); □I. *R. bisecta* < 10 µm (metre 59.2); □J. *R. bisecta* > 10 µm (metre 70.3); □K. *R. umbilica* (metre 109.5); □L–M. *Discoaster kuepperi* (metre 3); □N. *D. barbadiensis* (metre 107.5); □O. *D. sublodoensis* (metre 13.6); □P. *D. bifax* (metre 105.5); □Q. *Nannotetrina pappii* (metre 105.5); □R. *N. cristata* (metre 13.6). □S. *Tribrachiatus orthostylus* (metre 13.6); □T. *Toweius otzunali* (metre 3); □U. *Chiasmolithus solitus* (metre 82.5); □V. *N. fulgens* (metre 50.5); □W. *D. lodoensis* (metre 51.5); □X. *Chiasmolithus gigas* (metre 76.7). The scale bars are always 5 µm for smaller images (A to U) and 10 µm for larger images (V to X).

Zones CP12a and CP12b might be subjected to some uncertainties, as observed in many other sections (Backman 1986; Agnini *et al.* 2006). From metre 33 onwards, *B. inflatus* becomes discontinuous all the way up to its LO at metre 50.5. This position coincides with the FO of *Nannotetrina fulgens*, which marks the base of CP13a in a position within R2 preceding the FO of *G. nuttalli*. From this position onwards, *N. fulgens* appears to be very discontinuous until its disappearance in the uppermost part of the section. *Chiasmolithus gigas* is rare but appears continuously from metres 59.2 to 104.5. These positions are therefore taken as the base of Zone CP13b and of Zone CP13 c, which are located within R2 and N3, respectively. The last 6.5 m of the studied section are characterized by the presence of *R. umbilicus* > 14 μm. This enables the identification of the base of Subzone CP14a at metre 108.5, approximately at the boundary between N3 and R3.

In addition to these events, several additional first and last occurrences have also been recorded at the Agost section. The FRO of *R. bisecta* (specimens < 10 μm) has been recorded at metre 8.6 in the upper part of Subzone CP12a. The abundance of *R. bisecta* (< 10 μm) is always very variable throughout the section, although it becomes continuous from the uppermost part of CP12b upwards and is more abundant from CP13b until the top of the section. The FO of *R. bisecta* (> 10 μm) has been observed at metre 62.3. The occurrence of *R. bisecta* (> 10 μm), which is discontinuous for most of its range, is mainly linked to higher abundances of *R. bisecta* (< 10 μm). The FOs of *R. bisecta* (> 10 μm) and *R. scrippsae* are observed much earlier than previous estimates (Backman 1987), but agree with the results of Mita (2001) from ODP Hole 1051A (Blake Nose, NW Atlantic Ocean) and Agnini *et al.* (2006) from Posagno, Italy. The LO of *Coccolithus crassus* has been observed within Subzone CP12a. Moreover, the LO of *D. kuepperi* has been recognized at metre 13.6, in the lowermost part of CP12a in agreement with results by Martini & Müller (1986) and Sugarman *et al.* (2005). *Sphenolithus furcatolithoides* has its first but discontinuous occurrence in the upper part of Subzone CP12b, at metre 42.5, and it is continuously present from metre 71.5 onwards. The LO of *D. sublodoensis* has been observed near the top of Subzone CP12b at metre 45. A new taxon described by Bown (2005) in Tanzania, *B. globosus*, has been identified between metres 59.2 and 71.5.

An increase in abundance of *Sphenolithus*, *Discoaster barbadiensis* and *Ericsonia formosa* (warm-water taxa, Monechi *et al.* 2000), together with a maximum species richness, has been observed at the level with planktic foraminifera *C. eocaenica* and *C. Jarvisi* (metre 81.7), confirming an increase of sea surface temperature. Soon after, an increase in pentaliths, which are indicators of low salinity and high nutrient conditions (Bukry 1974; Kelly *et al.* 2003), together with a significant increase in the number of turbidite levels in the section between metres 81.7 and 86, suggests enhanced continental weathering and run-off.

Larger benthic foraminifera

Larger benthic foraminifera from the Agost section show very rich and diverse associations (see also Isuman 1983). Larger benthic foraminifera are displaced from their original habitat, but evidence of resedimentation phenomena or mixture of specimens from different ages has not been observed. Nummulitids are the most common larger benthic foraminifera, although in certain levels other larger foraminifera (orthophragminids) typical of open marine platforms have also been observed. Nummulitid specimens are, in general, well preserved, which has facilitated identification of most specimens at the species level. Systematic study of nummulitids has allowed us to recognize all the nummulitid biozones defined by Serra-Kiel *et al.* (1998) between the Early Eocene (middle Ypresian) and the Middle Eocene (middle Lutetian 2) (Figs 7, 8).

The first sample (metre 2, within N1) is characterized by *Nummulites cantabricus*, *Assilina laxispira* and *A.* aff. *placentula*, which are characteristic of Zone SBZ11. This sample also contains *N. leupoldi* and *N. irregularis* (typical of SBZ10 to 12), *N. pustulosus*, *N. escheri*, *N. partschi* and *A. marinellii* (typical of SBZ10 and 11), and *N. pratti* (which spans from SBZ11 to 12). The second sample (metre 15.7, within R1) includes *N. cantabricus*, *A. laxispira*, *N.* aff. *campesinus* and *A.* aff. *cuvillieri* (typical of SBZ11), *N. leupoldi* and *N. tauricus* (characteristic of SBZ10 to 12), *N. escheri*, *N. tenuilamellatus*, *A. escheri* and *A. marinellii* (SBZ10 and 11), and *N. pratti*, *N.* gr. *nemkovi-kaufmanni*, *N. bakhchisaraiensis* and *N.* aff. *nitidus*, (SBZ11 and 12). These associations are typical of the uppermost part of SBZ11.

The sample located at metre 30.4 (within N1) contains a nummulitid association characteristic of SBZ12. It contains *N. campesinus*, *A. maior*, *A. cuvillieri* and *A.* aff. *praespira*, (SBZ12), *N. leupoldi* (SBZ10 to 12), *N. pratti*, (SBZ11 and 12), and *N. praelorioli*, *N.* aff. *obesus*, *N. polygyratus*, *N. formosus*, *N.* aff. *irregularis*, *A. suteri* and *A.* aff. *escheri* (SBZ12 and 13).

The next sample (metre 36.7, base of R2) is characterized by the occurrence of *N. gallensis*, *Assilina* aff. *maior*, *A. spira abrardi*, *A.* aff. *tenuimarginata* and *A.* sp. aff. *escheri* (SBZ13), and *N. praelorioli*, *N. polygyratus*, *N. formosus*, *N.* aff. *irregularis*, *N.* sp.

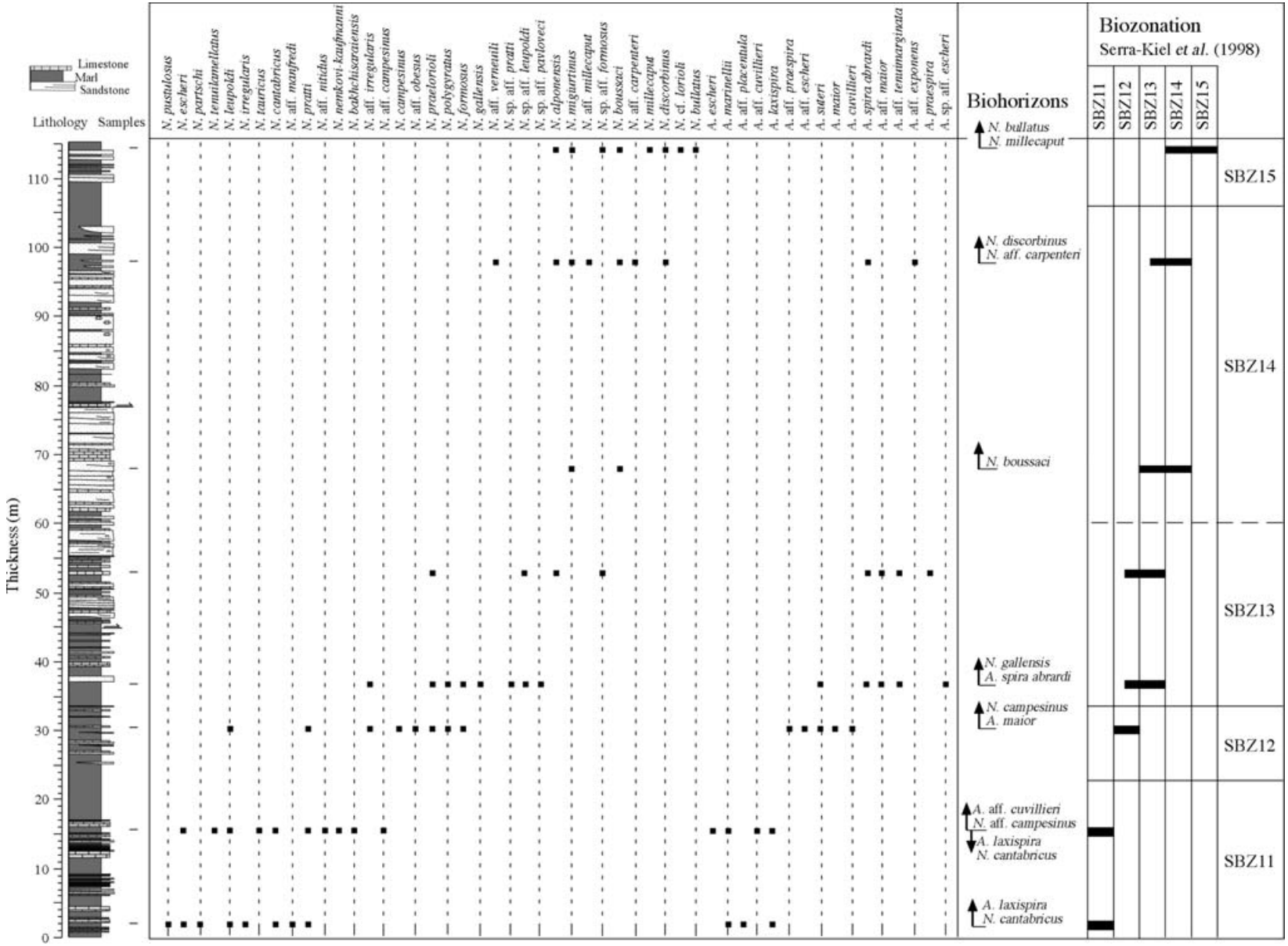

Fig. 7. Stratigraphic distribution of relevant larger benthic foraminifera and biozonation of the Agost section. The position of the studied samples is plotted against the stratigraphic log of the section. The boundary between SBZ zones is plotted halfway between samples assigned to two consecutive zones. Dashed line between SBZ13 and 14 denotes uncertainty in the determination of *N. boussaci* in the sample at metre 68.

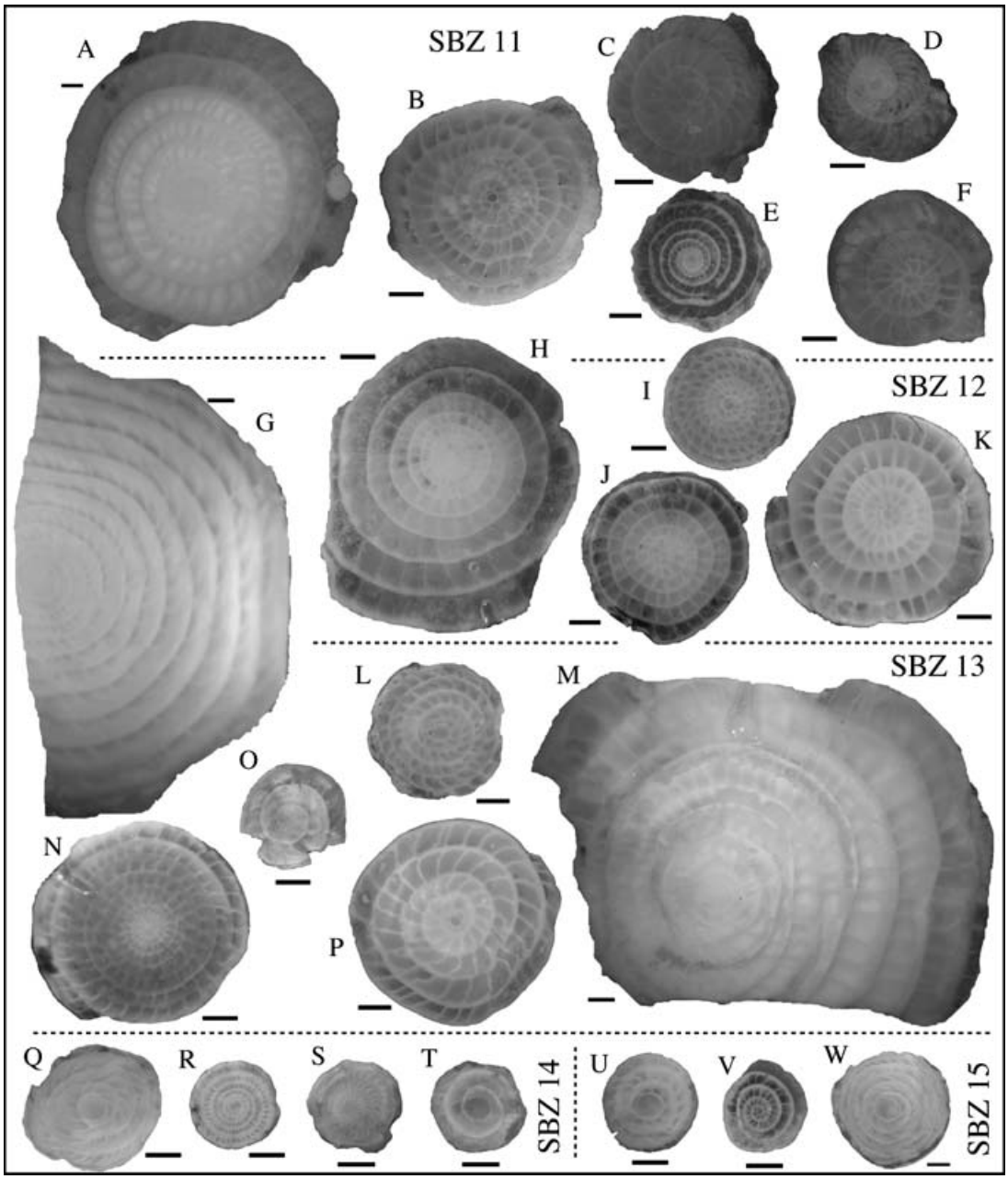

Fig. 8. Images of selected larger benthic foraminifera from the Agost section. ☐A. *Assilina laxispira*, B-form (metre 2); ☐B. *A. laxispira*, A-form (metre 2); ☐C. *Nummulites pratti*, A-form (metre 2); ☐D. *N. irregularis*, A-form (metre 2); ☐E. *N. cantabricus*, B-form (metre 2); ☐F. *A. marinellii*, A-form (metre 2); ☐G. *N. praelorioli*, B-form (metre 30.4); ☐H. *A. cuvillieri*, B-form (metre 30.4); ☐I. *N. campesinus*, A-form (metre 30.4); ☐J. *A. cuvillieri*, A-form (metre 30.4); ☐K. *A. maior*, A-form (metre 30.4); ☐L. *N. gallensis*, A-form (metre 36.7); ☐M. *A. spira abrardi*, B-form (metre 36.7); ☐N. *N. gallensis*, B-form (metre 36.7); ☐O. *N. alponensis*, A-form (metre 53); ☐P. *A.* aff. *maior*, A-form (metre 53); ☐Q. *N.* aff. *millecaput*, A-form (metre 98); ☐R. *N. discorbinus*, A-form (metre 98); ☐S. *N. migiurtinus*, A-form (metre 114.5); ☐T. *N.* cf. *boussaci*, A-form (metre 68); ☐U. *N.* cf. *lorioli*, A-form (metre 114.5); ☐V. *N. bullatus*, A-form (metre 114.5); ☐W. *N. millecaput*, A-form (metre 114.5). Scale bars = 1 mm.

aff. *pratti*, *N.* sp. aff. *leupoldi* and *N.* sp. aff. *pavloveci* (SBZ12 to 13). This association can be assigned to the lowermost zone of the Lutetian (SBZ13). The sample located at metre 53 (within R2) is characterized by nummulitid species that are also typical of SBZ13. It contains *Nummulites* sp. aff. *formosus*, *Assilina* aff. *maior*, *A. spira abrardi*, *A.* aff. *tenuimarginata* and *A. praespira* (characteristic of SBZ13), *N. praelorioli* and *N.* sp. aff. *leupoldi* (typical of SBZ12 and 13), and *N. alponensis* (SBZ13 and 14).

The next sample (metre 68, within R2) is characterized by a poor assemblage in which only some

specimens of *N. migiurtinus,* and some megalospheric specimens that might be attributed to *N. boussaci*, are found. Based on the biostratigraphic range of these species, this sample has been tentatively attributed to SBZ 14. The sample located at metre 98 (within N3) presents a rich nummulitid association characterized by *N. boussaci* and *N.* aff. *carpenteri* (SBZ14), *N. alponensis*, *N.* aff. *millecaput*, *N.* aff. *verneuili*, *N. obesus-hilarionis* and *Assilina* aff. *exponens* (biostratigraphic range spanning SBZ13 to 14), and *N. discorbinus* (SBZ14 to 16). This assemblage is typical of SBZ 14.

The uppermost sample (metre 114.5, within R3) contains *N. bullatus* and *N.* sp. aff. *formosus* (SBZ15 and 16), *N. millecaput*, *N. discorbinus* and *N.* cf. *lorioli (*which span Zones SBZ14 to 16), and *N. alponensis* and *N. migiurtinus* (characteristic of SBZ13 and 14). This association can be assigned to SBZ15.

Small benthic foraminifera

The small benthic foraminiferal assemblages of the Agost section are diverse and dominated by calcareous taxa (Figs 9, 10). The most common calcareous species are *Bolivinoides crenulata*, *Cibicidoides eocaenus*, *Anomalinoides acutus*, *Hanzawaia ammophila*, *Osangularia plummerae*, and *Globocassidulina subglobosa*. The agglutinated foraminiferal assemblages are dominated by cylindrical tapered genera such as *Clavulinoides*, *Gaudryina*, and *Pseudoclavulinoides* (Fig. 10). *Nuttallides truempyi*, *Oridorsalis umbonatus*, *Bulimina trinitatensis*, and *Buliminella grata* are present but not abundantly, whereas *C. eocaenus*, *H. ammophila*, *A. acutus*, uniserial calcareous species, *Oridorsalis*, *Lenticulina*, *Uvigerina*, and *Clavulinoides* are common throughout the studied section. Reworked shallow-water taxa such as *Asterigerina* or *Pararotalia*, which are considered allochthonous, were also identified. Most Eocene deep-water species generally have long stratigraphic ranges (Tjalsma & Lohmann 1983; Thomas 1990) and, therefore, assignation of the studied samples to benthic bathyal zones of Berggren & Miller (1989) is not straightforward. Among other species present throughout the section, *H. ammophila* and *N. truempyi* are characteristic of Zones BB2 and BB3. Unfortunately, the marker for the base of Zone BB3, *Cibicidoides subspiratus*, has not been identified in the Agost section. Nevertheless, the BB2/BB3 boundary can be tentatively located at around metre 65, which is the level at which the occurrence of *N. truempyi* becomes common and where the LO of *Loxostomoides applini* is found.

Small benthic foraminifera might provide palaeoenvironmental estimates (e.g. Tjalsma & Lohmann 1983). *Aragonia aragonensis* has a peak in abundance at metre 86, few metres above the FO of *H. nuttalli.* This might indicate that the P9/P10 boundary was associated with a hyperthermal event, as also suggested in the Fortuna section (Molina *et al.* 2006). This is consistent with the occurrence of planktic foraminifera *C. eocaenica* and *C. jarvisi*, and of calcareous nannofossils *Sphenolithus*, *Discoaster barbadiensis* and *Ericsonia Formosa*, just before the FO of hantkeninids, which provide compelling evidence for an excursion of tropical species due to an increase in seawater temperature.

Discussion

Integrated magnetobiostratigraphy of the Agost section

Correlation of the magnetic stratigraphy from Agost to the GPTS is based on the position of relevant biostratigraphic horizons in light of recent results from the Gorrondatxe (Bernaola *et al.* 2006; Payros *et al.* 2007) and Possagno (Agnini *et al.* 2006) sections, and also from a revised magnetobiostratigraphy of the Middle Eocene interval of the Contessa section (Jovane *et al.* 2007) (Fig. 11). In Gorrondatxe and Possagno, the FRO of *D. sublodoensis*, and hence the base of CP12a, is located within Chron C22n. At Agost, the FRO of *D. sublodoensis* is located within N1, which can therefore be correlated to Chron C22n (Fig. 11A). The FO of *B. inflatus*, which has not been identified at Possagno, is located in the middle part of Chron C21r in Gorrondatxe. At Agost, the FO of *B. inflatus* is located within R1, which can therefore be unambiguously correlated to Chron C21r despite its somehow unclear alternation of normal and reverse polarity samples. This interpretation implies that N2 correlates to Chron C21n, and that N3 correlates to Chron C20n. R2 would therefore correlate to Chron C20r, and R3 to Chron C19r. This correlation implies highest sedimentation rates within Chron C20r, which is entirely consistent with the predominance of turbidites in the middle part of the section, and agrees with the resulting calibration of other relevant biostratigraphic events in the section. Thus, FO of *C. gigas*, which lies in the lower-middle part of R2 at Agost, is located near the base of Chron C20r in Gorrondatxe, Possagno, and Contessa. Similarly, the FO of *R. umbilicus* > 14 μm, which occurs at the N3/R3 boundary at Agost, is correlated to the C20n/C19r boundary at Contessa (Jovane *et al.* 2007). It should also be noticed that the FOs of *G. nuttalli* and *H. nuttalli*, which are located in the lower and upper part of R2 (C20r) at Agost, respectively, are

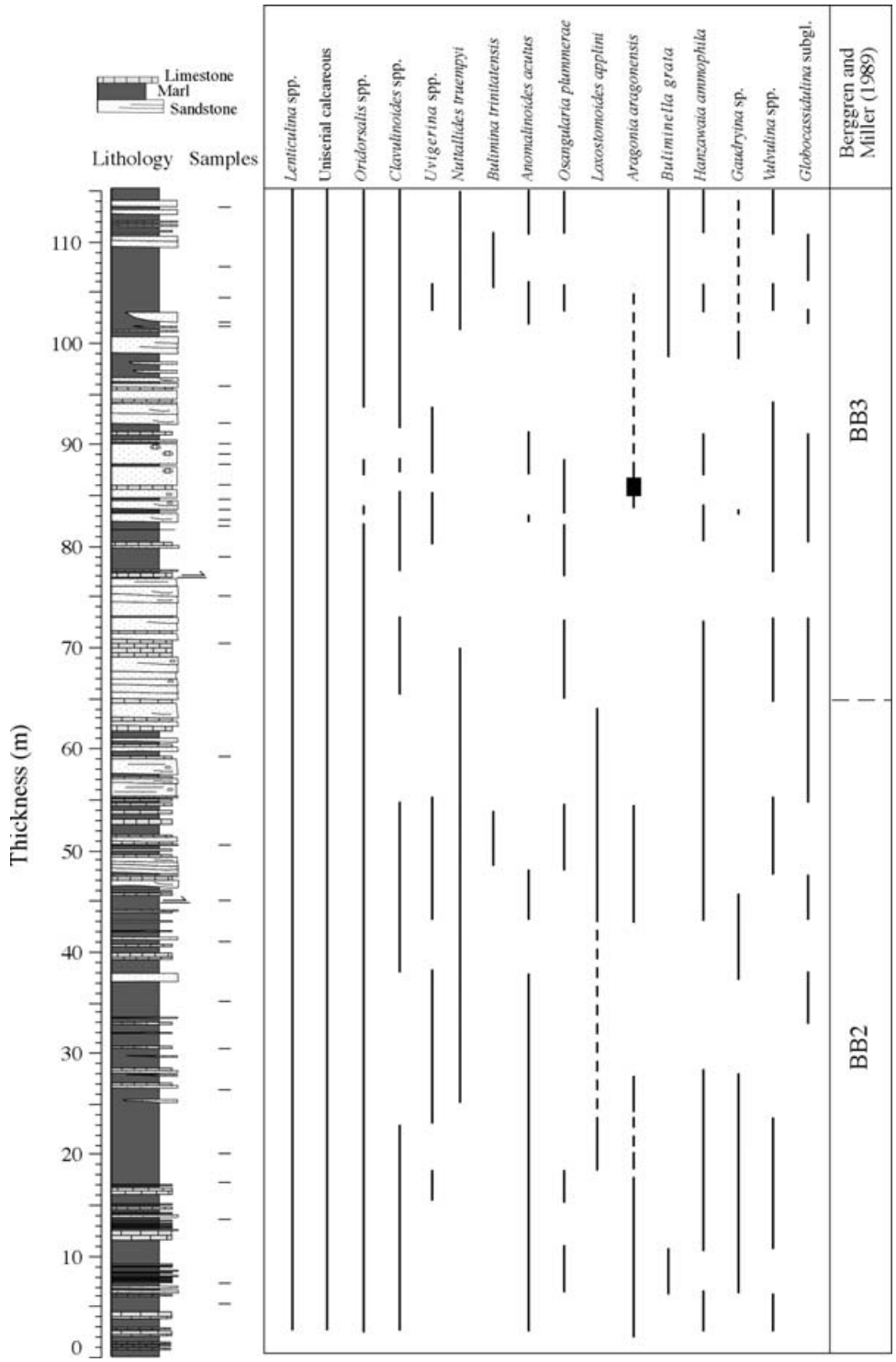

Fig. 9. Stratigraphic distribution of relevant small benthic foraminifera and biozonation of the Agost section. The position of the studied samples is plotted against the stratigraphic log of the section.

located at a very similar position within Chron C20r at Gorrondatxe. This indicates that, contrary to previous interpretations (e.g. Bernaola *et al.* 2006), the FOs of *G. nuttalli* and *H. nuttalli* occur rather synchronously in the Betic (Tethys) and Pyrenean (North Atlantic) domains.

The solution proposed for the Agost section results in a correlation between calcareous nannofossil zones

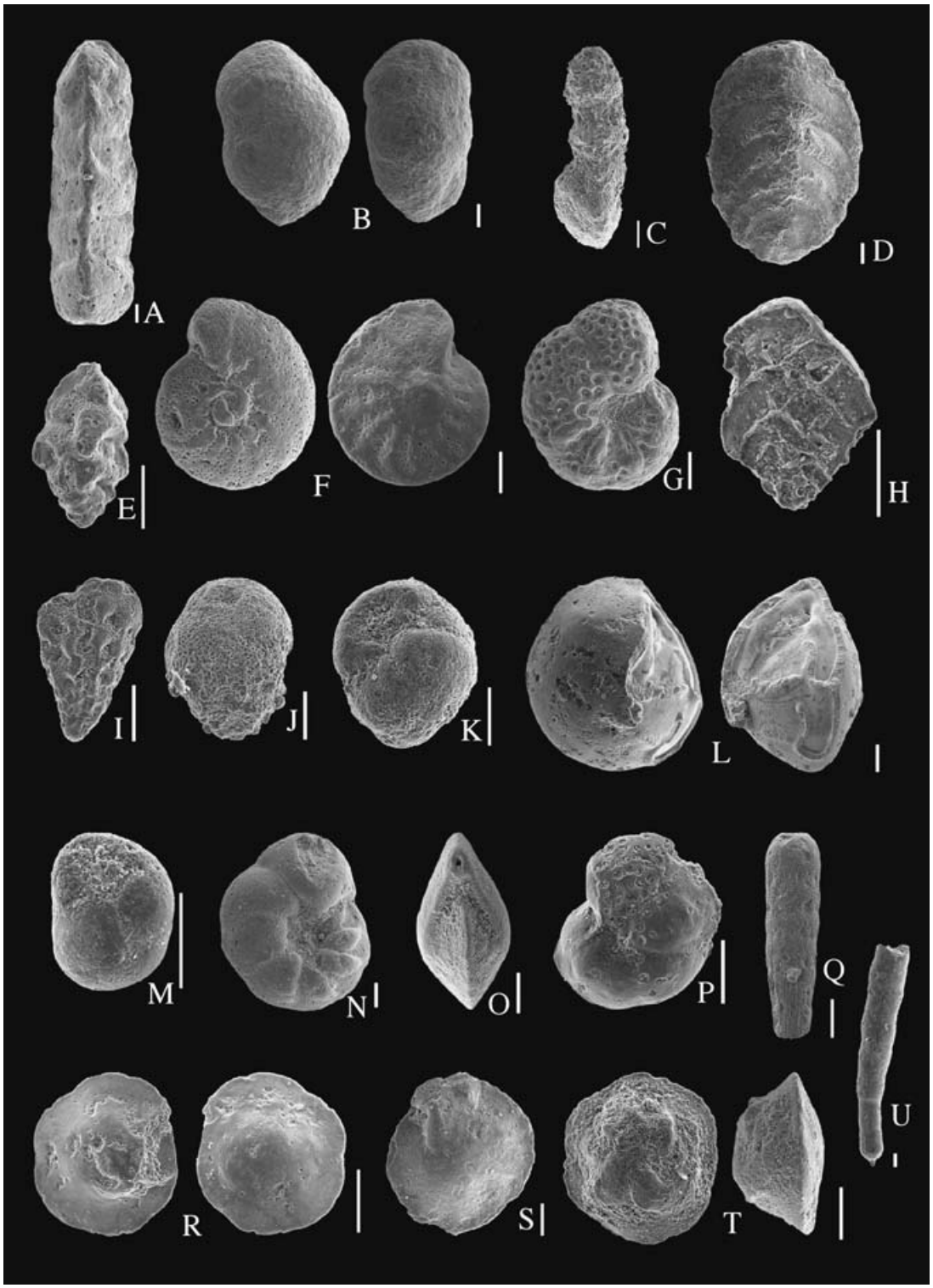

Fig. 10. Scanning electron microscope images of selected small benthic foraminifera from the Agost section. ☐A. *Clavulinoides angularis* (metre 82); ☐B. *Gaudryina* sp. (metre 84.5); ☐C. *Pseudoclavulina* sp. (metre 26.4); ☐D. *Vulvulina* sp. (metre 82); ☐E. *Angulogerina muralis* (metre 82); ☐F. *Anomalinoides acutus* (metre 90); ☐G. *A. capitatus* (metre 5.3); ☐H. *Aragonia aragonensis* (metre 84.5); ☐I. *Bolivinoides crenulata* (metre 82.5); ☐J. *Bulimina trinitatensis* (metre 102); ☐K. *Buliminella grata* (metre 101.7); ☐L. *Cibicidoides naranjoensis* (metre 84.5); ☐M. *Globocassidulina subglobosa* (metre 92); ☐N. *Hanzawaia ammophila* (metre 82); ☐O. *Lenticulina* sp. (metre 88); ☐P. *Lobatula lobatula* (metre 92); ☐Q. *Loxostomoides applini* (metre 82); ☐R. *Oridorsalis umbonatus* (metre 82); ☐S. *Osangularia plummerae* (metre 82); ☐T. *Nuttallides truempyi* (metre 101.7); ☐U. *Siphonodosaria annulifera* (metre 84.5). Scale bars = 100 μm.

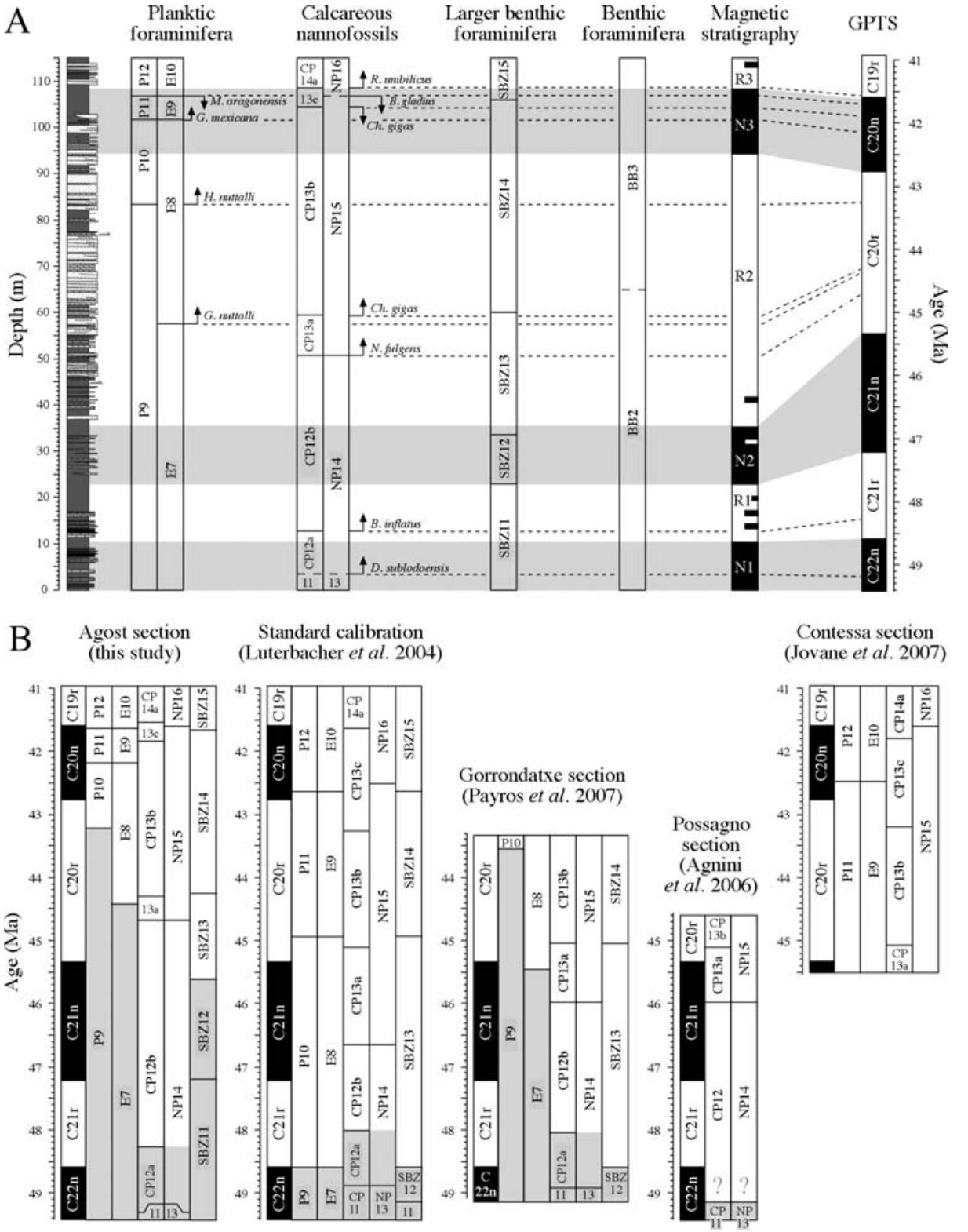

Fig. 11. □A. Correlation of the Agost section with the revised geomagnetic polarity timescale (GPTS) of Luterbacher *et al.* (2004). Absolute ages for bioevents in Agost have been calculated by converting their stratigraphic distance to the closest polarity reversal into time, assuming a constant sedimentation rate between successive polarity reversals around each bioevent. □B. Comparison of results from Agost (this study), Gorrondatxe (Payros *et al.* 2007), Possagno (Agnini *et al.* 2006), Contessa (Jovane *et al.* 2007), and standard biozonation schemes placed on the revised GPTS scale (Luterbacher *et al.* 2004). The boundary between the grey (Ypresian) and white (Lutetian) bars indicates the location of the Ypresian/Lutetian boundary according to different fossil groups. In Possagno, the absence of the marker of CP12a prevents accurate delineation of the boundary.

and magnetic polarity chrons that provides an overall good match with standard magnetobiostratigraphic calibration schemes (Berggren *et al.* 1995; Luterbacher *et al.* 2004) (Fig. 11B), and is consistent with independent results from Gorrondatxe, Possagno and Contessa. The only differences correspond to the base of calcareous nannofossil Zones NP15/CP13 and CP13c, whose anomalously late positions at Agost might be explained by the rare and discontinuous occurrence of *Nannotetrina* and the likely extended range of *Ch. gigas* in shelf settings (Pearson *et al.* 2004). In contrast, the correlation proposed for the Agost section introduces a major shift in the standard calibration of planktic foraminiferal Zones P10/E8 to P12/E10 (Fig. 11B). Thus, the FOs of *H. nuttalli* and *G. nuttalli* do not occur simultaneously near the C22n/C21r boundary, as have also been noticed in Gorrondatxe and other sections (Payros *et al.* 2007), but at a much younger and diachronous age within Chron C20r (ca. 43.2 and ca. 44.6 Ma, respectively). Moreover, the LO of *M. aragonensis* does not occur in the lower part of C20n, but at a younger age at the uppermost part C20n. Finally, it should also be noted that the correlation proposed for the Agost section also introduces a shift in the standard calibration of larger benthic foraminiferal Zones SBZ12 and 13 (Fig. 11B).

Implications for the Ypresian/Lutetian boundary

Definition of any GSSP requires the selection of a marker event in a rock sequence. Such marker event should be chosen from a bundle of successive events in order to enable widespread recognition of the chronostratigraphic boundary in the absence of the primary marker (Remane *et al.* 1996). In the case of the Ypresian/Lutetian boundary, the bundle of potential markers includes the FO of *B. inflatus* (base of CP12b), the SBZ12/SBZ13 boundary, the FO of *G. nuttalli* (base of E8), the FO of *H. nuttalli* (base of P10), and the C22n/C21r boundary. Noticeably, all these events are represented in the Agost section. The FO of *B. inflatus* (base of CP12b) is found at metre 13.2, in the lower part of Chron C21r. The boundary between shallow benthic Zones SBZ12 and SBZ13 is located at about metre 34, in the uppermost part of Chron C21n. The FO of *G. nuttalli* is located at metre 57, in the lower part of Chron C20r. The FO of *H. nuttalli* is found higher up in the section, at metre 83.6 near the top of Chron C20r. This sequence of events found in Agost shows remarkable similarities, and also some discrepancies, with the sequence of events described in other sections (Fig. 11B). Both at Agost and at Gorrondatxe, the FO of *B. inflatus* (base of CP12b) is located in the lower part of Chron C21r. These results are compatible with the base of CP12 near the C22n/C21r boundary at Possagno, where the FO of *B. inflatus* (base of CP12b) could not be identified. The boundary between shallow benthic Zones SBZ12 and SBZ13 appears to be younger in Agost, where it is located near the C21n/C20r boundary, than in Gorrondatxe, where it is located at the boundary between Chrons C22n and C21r. The FO of *G. nuttalli* (base of E8) seems to be only slightly younger in Agost (lowermost part of C20r) than in Gorrondatxe (uppermost part of C21n), whereas the FO of *H. nuttalli* (base of P10) is located at a very similar position (upper part of C20r) in both sections. The remarkable good match in the delayed position of Zones E8 and P10 as derived from Agost and Gorrondatxe contrasts with new results from Contessa, where Zone P10/E8 must pre-date Chron C20r (Fig. 11B) (Jovane *et al.* 2007). Since *G. nuttalli* and *H. nuttalli* are frequently rare outside the tropical belt, it might be argued that a possible delayed apparition of these species at Agost and Gorrondatxe could be caused by environmental factors. Similarly, the delayed position of the base of Zones P11/E9 and P12/E10 might also be due to environmental factors or to reworking. A recent compilation of magnetobiostratigraphic results from 13 stratigraphic sections distributed worldwide, including Gorrondatxe, has unequivocally demonstrated that the boundary between planktic foraminiferal Zones P9/P10 occurs systematically close to the boundary between calcareous nannofossil Zones CP12/CP13 (NP14/NP15) and Chrons C21n/C20r, and not within Subzone CP12a (lower part of NP14) near the C22n/C21r boundary (Payros *et al.* 2007) as might be derived from Contessa (Jovane *et al.* 2007). Given this compelling evidence, and in view of the difficulties in the identification of planktic foraminifera in sections of the Gubbio area (Lowrie *et al.* 1982; Napoleone *et al.* 1983; Opdyke & Channell 1995), we consider that consistent magnetobiostratigraphic solutions from Agost and Gorrondatxe provide reliable results concerning the age of plaktic foraminiferal events. In that case, standard calibration schemes of planktic foraminiferal Zones P10/E8 and P11/E9 might need to be modified, which bears important implication for the definition of the Ypresian/Lutetian boundary since two of the possible markers of the boundary are based on planktic foraminifera events.

For the sake of continuity, either the FO of *H. nuttalli* (base of P10) or the FO of *G. nuttalli* (base of E8) might be chosen as a primary marker of the Ypresian/Lutetian boundary. The hyperthermal event associated to the FO of *H. nuttalli* might help in identifying the boundary if this datum was

selected as the primary marker. In any case, the age of the boundary would be much younger (3–5 Myr) than hitherto considered (Fig. 11B). Alternatively, the Ypresian/Lutetian boundary might be chosen at the boundary between larger benthic foraminiferal Zones SBZ12/SBZ13, or at the FO of *B. inflatus* (base of CP12b). In view of the results obtained from the Agost section, and keeping in mind the results from other sections elsewhere (Payros *et al.* 2007), it is apparent that the FO of *B. inflatus* (base of CP12b, lower part of C21r) is the only potential biostratigraphic marker event of the Ypresian/Lutetian boundary that seems to be synchronous in most sections where reliable magnetobiostratigraphic results have been obtained. The choice of the base of CP12b as a primary marker of the Ypresian/Lutetian boundary would also fit with the age of the base of the Lutetian stratotype in the Paris basin, which has been correlated to Zone NP14 (Berggren *et al.* 1995). This would result in an age for the Ypresian/Lutetian boundary of around 48.2 Ma, similar to that proposed in revised standard calibration schemes (Luterbacher *et al.* 2004; Berggren & Pearson 2005, 2006; Pearson *et al.* 2006a) (Fig. 11B).

Conclusions

The integrated magnetobiostratigraphic study presented in this paper provides conclusive evidence that the Agost section is continuous and spans from Zones P9 to P12 (E7 to E10), Zones CP11 to CP14a (NP13 to NP16), Zones SBZ11 to SBZ15, and Chrons C22n to C19r (Fig. 11). The results obtained in the Agost section indicate that, in agreement with the work of Bernaola *et al.* (2006) at the Gorrondatxe section, all the events that have traditionally been proposed to mark the Ypresian/Lutetian boundary appear at different stratigraphic levels. Thus, the FO of *H. nuttalli* (base of P10) and the FO of *G. nuttalli* (base of E8) are found within Chron C20r, at a much younger age (3–5 Myr) than previously considered in standard calibration schemes (Berggren *et al.* 1995; Luterbacher *et al.* 2004; Berggren & Pearson 2005, 2006; Pearson *et al.* 2006a). Similarly, the boundary between SBZ12 and SBZ13 is located within Chron C21n, also at a younger position than previously considered (see Serra-Kiel *et al.* 1998; Luterbacher *et al.* 2004). On the contrary, the FO of *B. inflatus* (base of CP12b) is found within Chron C21r, which conforms to the magnetostratigraphically calibrated age of ca. 48 Ma (middle part of C21r) considered in standard calibration schemes (Berggren *et al.* 1995; Luterbacher *et al.* 2004; Berggren & Pearson 2005, 2006; Pearson *et al.* 2006a). Of all the potential biostratigraphic markers of the Ypresian/Lutetian boundary, the choice of the FO of *B. inflatus* (base of CP12b) as a marker of the boundary might be the best option.

In view of the results presented in this paper, the Agost section can be proposed as a suitable candidate to locate the GSSP for the Ypresian/Lutetian boundary because it fulfils most of the geological, biostratigraphic and accessibility requirements that any prospective GSSP should meet (see Remane *et al.* 1996): (i) it has a relatively high sedimentation rate, it is demonstrably continuous despite the presence of some turbidite deposits, and it is exposed over an adequate thickness of sediments; (ii) it includes diverse and well-preserved fossil groups, and enables the selection of the primary marker event from a bundle of well dated biostratigraphic events; and (iii) it is easily accessible and offers the possibility for protection of a permanent marker.

Acknowledgements. – This research was supported by projects CGL2004-00738 (MEC, Spain) and Group E05 (Gobierno de Aragón). JCL benefits from a Ramón y Cajal contract (MEC) and SO from a Gobierno de la Rioja PhD fellowship. SM and FT were supported by project MIUR/PRIN COFIN 2005. We thank Aitor Payros and an anonymous reviewer, whose detailed and thoughtful comments greatly improved an earlier version of this manuscript, and Svend Stouge for his help with editorial handling.

References

Agnini, C., Muttoni, G., Kent, D.V. & Rio, D. 2006: Eocene biostratigraphy and magnetic stratigraphy from Possagno, Italy: The calcareous nannofossil response to climate variability. *Earth and Planetary Science Letters 241*, 815–830.

Alonso-Zarza, A.M., Armenteros, A., Braga, J.C. *et al.* 2002: Tertiary. *In* Gibbons, W. & Moreno, T. (eds): *The Geology of Spain*. Geological Society, 293–334.

Aubry, M.P. 1995: From chronology to stratigraphy: interpreting the Lower and Middle Eocene stratigraphic record in the Atlantic ocean. *In* Berggren, W.A., Kent, D.V., Aubry, M.P. & Hardenbol, J. (eds): *Geochronology, Time Scales and Global Stratigraphic Correlation*. Society of Economic Paleontologists and Mineralogists (SEPM) (Society for Sedimentary Geology) Special Publication No. 54, 213–274. SEPM, Tulsa, OK.

Backman, J. 1986: Late Paleocene to middle Eocene calcareous nannofossil biochronology from the Shatsky Rise, Walvis Ridge and Italy. *Palaeogeography, Palaeoclimatology, Palaeoecology 57*, 43–59.

Backman, J. 1987: Quantitative calcareous nannofossil biochronology of middle eocene through early oligocene sediment from DSDP sites 522 and 523. *Abhandlungen der Geologischen Bundes Anstalt* (Wien), Bd. *39*, 21–31.

Berggren, W.A. & Miller, K.G. 1989: Cenozoic bathyal and abyssal calcareous benthic foraminiferal zonation. *Micropalentology 35*, 308–320.

Berggren, W.A. & Pearson, P.N. 2005: A revised tropical to subtropical Paleogene planktonic foraminiferal zonation. *Journal of Foraminiferal Research 35*, 279–298.

Berggren, W.A. & Pearson, P.N. 2006: Tropical to subtropical planktonic foraminiferal zonation of the Eocene and Oligocene. *In* Pearson, P.N., Olsson, R.K., Huber, B.T., Hemleben, C. & Berggren, W.A. (eds): *Atlas of Eocene Planktonic Foraminifera*, 29–40. Cushman Foundation Special Publication No. 41, Smithsonian Institution, Washington, DC.

Berggren, W.A., Kent, D.V., Swisser, C.C. & Aubry, M.P. 1995: A revised Cenozoic geochronology and chronostratigraphy. *In* Berggren, W.A., Kent, D.V., Aubry, M.P. & Hardenbol, J. (eds): *Geochronology, Time Scales and Global Stratigraphic Correlation*. Society of Economic Paleontologists and Mineralogists (SEPM) (Society for Sedimentary Geology) Special Publication No. 54, 129–212. SEPM, Tulsa, OK.

Bernaola, G., Orue-Etxebarria, X., Payros, A., Dinarès-Turell, J., Tosquella, J., Apellaniz, E. & Caballero, F. 2006: Biomagnetostratigraphic analysis of the Gorrondatxe section (Basque Country, Western Pyrenees): Its significance for the definition of the Ypresian/lutetian boundary stratotype. *Neues Jahrbuch für Geologie und Paläontologie Abhandlungen 241*, 67–109.

Bowles, J. 2006: Data report: Revised magnetostratigraphy and magnetic mineralogy of sediments from Walvis Ridge, Leg 208. *In* Kroon, D., Zachos, J.C. & Richter, C. (eds): *Proceedings of the Ocean Drilling Program, Scientific Results 208*, 1–24, College Station, TX (Ocean Drilling Program).

Bown, P.R. 2005: Paleogene calcareous nannofossils from the Kilwa and Lindi areas of coastal Tanzania: Tanzania Drilling Project Sites 1 to 10. *Journal of Nannoplankton Research 27*, 21–95.

Bukry, D. 1974: Coccoliths as paleosalinity indicators: Evidence from Black Sea. *American Association of Petroleum Geologists Memoir 20*, 353–363.

van Fossen, M.C. 1997: Magnetostratigraphy of lower Eocene to lower Miocene sediments in cores from the New Jersey coastal plain. *In* Miller, K.G. & Snyder, S.W. (eds): *Proceedings of the Ocean Drilling Program, Scientific Results 150X*, 295–304. College Station, TX (Ocean Drilling Program).

Galbrun, B. 1992: Magnetostratigraphy of Upper Cretaceous and Lower Tertiary sediments, Sites 761 and 762, Exmouth Plateau, northwest Australia. *In* von Rad, U. & Haq, B.U. (eds): *Proceedings of the Ocean Drilling Program, Scientific Results 122*, 699–717. College Station, TX (Ocean Drilling Program).

Geel, T. 2000: Recognition of stratigraphic sequences in carbonate platform and slope deposits: empirical models based on microfacies analysis of Paleogene deposits in southeastern Spain. *Palaeogeography, Palaeoclimatology, Palaeoecology 155*, 211–238.

Gonzalvo, C. & Molina, E. 1998: Planktic foraminiferal biostratigraphy across the Lower-Middle Eocene transition in the Betic Codillera (Spain). *Neues Jahrbuch für Geologie und Paläontologie Monatshefte 11*, 671–693.

Gradstein, F.M., Ogg, J.G. & Smith, A. (eds), 2004: *A Geologic Time Scale 2004*, 589 pp. Cambridge University Press, Cambridge, UK.

Groot, J.J., De Jonge R.B.G., Langereis, C.G., Tenkate, W.G.H.Z. & Smit, J. 1989: Magnetostratigraphy of the Cretaceous Tertiary boundary at Agost (Spain). *Earth and Planetary Science Letters 94*, 385–397.

Guerrera, F., Estévez, A., López-Arcos, M., Martín-Martín, M., Martin-Pérez, J.A. & Serrano, F. 2006: Paleogene tectonosedimentary evolution of the Alicante Through (External Betic Zone, SE Spain) and its bearings on the timing of the deformation of the South-Iberian Margin. *Geodinamica Acta 19*, 87–101.

Isuman, N. 1983: Mikropaläontologische Untersuchungen von Großforami-niferen (Nummuliten und Assilinen) im Alttertiär von Südostspanien (Aspe und Agost in der Provinz Alicante). *Berliner Geowissenschaft Abhandlungen 49*, 61–170.

Jovane, L., Florindo, F., Coccioni, R., Dinarès-Turell, J., Marsili, A., Monechi, S., Roberts, A.P. & Sprovieri M. 2007: The middle Eocene climatic optimum event in the Contessa Highway section, Umbrian Apennines, Italy. *Geological Society of America Bulletin 119*, 413–427.

Kelly, D.C., Norris, R.D. & Zachos, J.C. 2003: Deciphering the paleoceanographic significance of Early Oligocene Braarudosphaera chalks in the South Atlantic. *Marine Micropaleontology 49*, 49–63.

Kirschvink, J.L. 1980: The least-squares line and plane in the analysis of palaeomagnetic data. *Geophysical Journal of the Royal Astronomical Society 62*, 699–718.

Lowrie, W., Alvarez, W., Napoleone, G., Perch-Nielsen, K., Premoli Silva, I.P. & Toumarkine, M. 1982: Paleogene magnetic stratigraphy in Umbrian pelagic carbonate rocks – The Contessa sections, Gubbio. *Geological Society of America Bulletin 93*, 414–432.

Luterbacher, H.P., Ali, J.R., Brinkhuis, H., Gradstein, F.M., Hooker, J.J., Monechi, S., Ogg, J.G., Powell, J., Röhl, U., Sanfilippo, A. & Schmitz, B. 2004: The paleogene period. *In* Gradstein, F.M., Ogg, J.G. & Smith, A. (eds): *A Geologic Time Scale 2004*, 384–408. Cambridge University Press, Cambridge, UK.

Martini, E. 1971: Standard Tertiary and Quaternary calcareous nannoplankton zonation. *In* Farinacci, A. (ed.): *Proceedings of the Second International Conference on Planktonic Microfossils Roma*, Tecnoscienza 2, 739–785.

Martini, E. & Müller, C. 1986: Current Tertiary and Quaternary calcareous nannoplankton stratigraphy and correlations. *Newsletters on Stratigraphy 16*, 99–112.

Mita, I. 2001: Data Report: Early to Late Eocene calcareous nannofossil assemblages of Sites 1051 and 1052, Blake Nose, northwestern Atlantic Ocean. *In* Kroon, D., Norris, R.D. & Klaus, A. (eds): *Proceedings of the Ocean Drilling Program, Scientific Results 171B*, 1–28. College Station, TX (Ocean Drilling Program).

Molina, E., Cosovic, V., Gonzalvo, C. & Von Salis, K. 2000: Integrated biostratigraphy across the Ypresian/Lutetian boundary at Agost, Spain. *Revue de Micropaleontologie 43*, 381–391.

Molina, E., Gonzalvo, C., Mancheño, M.A., Ortiz, S., Schmitz, B., Thomas, E. & Von Salis, K. 2006: Integrated stratigraphy and chronostratigraphy across the Ypresian-Lutetian transition in the Fortuna Section (Betic Cordillera, Spain). *Newsletters on Stratigraphy 42*, 1–19.

Monechi, S., Buccianti, A. & Gardin, S. 2000: Biotic signals from nannoflora across the iridium anomaly in the Upper Eocene of the Massignano section: evidence from statistical analyses. *Marine Micropaleontology 39*, 219–237.

Napoleone, G., Silva, I.P., Heller, F., Cheli, P., Corezzi, S. & Fischer, A.G. 1983: Eocene magnetic stratigraphy at Gubbio, Italy, and its implications for Paleogene geochronology. *Geological Society of America Bulletin 94*, 181–191.

Ogg, J.O. & Bardot, L. 2001: Aptian through Eocene magnetostratigraphic correlation of the Blake Nose transect (Leg 171B), Florida Continental Margin. In Kroon, D., Norris, R.D. & Klaus, A. (eds): *Proceedings of the Ocean Drilling Program, Scientific Results 171B*, 1–58. College Station, TX (Ocean Drilling Program).

Okada, H. & Bukry, D. 1980: Supplementary modification and introduction of code numbers to the low latitude coccolith biostratigraphic zonation (Bukry 1973, 1975). *Marine Micropaleontology 5*, 321–325.

Opdyke, N.D. & Channell, J.E.T. 1995: *Magnetic Stratigraphy*, 346 pp. Academic Press, San Diego, CA.

Payros, A., Bernaola, G., Orue-Etxebarria, X., Dinarès-Turell, J., Tosquella, J. & Apellaniz, E. 2007: Reassesment of the Early-Middle Eocene biomagnetochronology based on evidence from the Gorrondatxe section (Basque Country, western Pyrenees). *Lethaia 40*, 183–195.

Payros, A., Orue-Etxebarria., X. & Pujalte, V. 2006: Covarying sedimentary and biotic fluctuations in Lower-Middle Eocene Pyrenean deep-sea deposits: Palaeoenvironmental implications. *Palaeogeography, Palaeoclimatology, Palaeoecology 234*, 258–276.

Pearson, P.N., Nicholas, C.J., Singano, J.M., Bown, P.R., Coxall, H.K., van Dongen, B.E., Huber, B.T., Karega, A., Lees, J.A., Msaky, E., Pancost, R.D., Pearson, M. & Roberts, A.P. 2004: Paleogene and Cretaceous sediment cores from Kilwa and Lindi areas of coastal Tanzania: Tanzania Drilling Project Sites 1–5. *Journal of African Earth Sciences 39*, 25–62.

Pearson, P.N., Olsson, R.K., Huber, B.T., Hemleben, C. & Berggren, W.A. (eds), 2006a: *Atlas of Eocene Planktonic Foraminifera*, 513 pp. Cushman Foundation Special Publication No. 41, Smithsonian Institution, Washington, DC.

Pearson, P.N., Olsson, R.K., Huber, B.T., Hemleben, C., Berggren, W.A. & Coxall, H.K., 2006b: Overview of Eocene Planktonic foraminiferal taxonomy, paleoecology, phylogeny, and biostratigraphy. *In* Pearson, P.N., Olsson, R.K., Huber, B.T., Hemleben, C. & Berggren, W.A. (eds): *Atlas of Eocene Planktonic Foraminifera*, 11–28. Cushman Foundation Special Publication No. 41, Smithsonian Institution, Washington, DC.

Remane, J., Bassett, M.G., Cowie, J.W., Gohrbandt, K.H., Lane, R., Schulz, H., Michelsen, O. & Naiwen, W. 1996: Revised guidelines for the establishment of global chronostratigraphic standards by the International Commission on Stratigraphy. *Episodes 19*, 77–81.

Serra-Kiel, J., Hottinger, L., Caus, E., Drobne, K., Ferrández, C., Jauhri, A.K., Less, G., Pavlovec, R., Pignatti, J., Samsó, J.M., Schaub, H., Sirel, E., Strougo, A., Tambareau, Y., Tosquella, J. & Zakrevskaya, E. 1998: Larger foraminiferal biostratigraphy of the Tethyan Paleocene and Eocene. *Bulletin de la Societe Geologique de France 169*, 281–299.

Suganuma, Y. & Ogg, J.G. 2006: Campanian through Eocene magnetostratigraphy of Sites 1257–1261, ODP Leg 207, Demerara Rise (western equatorial Atlantic). *In* Mosher, D.C., Erbacher, J. & Malone, M.J. (eds): *Proceedings of the Ocean Drilling Program, Scientific Results 207*, 1–48, <http://www-odp.tamu.edu/publications/207_SR/102/102.htm>

Sugarman, P.J., Miller, K.G., Browning, J.V. *et al.* 2005: Millville site. *In* Miller, K.G., Sugarman, P.J. & Browning, J.V. (eds): *Proceedings of the Ocean Drilling Program, Initial Reports 174AX* (Suppl.), 94.

Thomas, E. 1990: Late Cretaceous through Neogene deep-sea benthic foraminifers (Maud Rise, Wedell Sea, Antarctica). *Proceedings of the Ocean Drilling Program, Scientific Results 113*, 571–594.

Thomas, E. 2003: Extinction and food at the sea floor: a high-resolution benthic foraminiferal record across the Initial Eocene Thermal Maximum, Southern Ocean Site 690. *In* Wing, S., Gingerich, P., Schmitz, B. & Thomas, E. (eds): *Causes and Consequences of Globally Warm Climates of the Paleogene*, Geological Society of America, Special Paper 369, 319–332.

Tjalsma, R.C. & Lohmann, G.P. 1983: Paleocene-Eocene bathyal and abyssal benthic foraminifera from the Atlantic Ocean. *Micropaleontology, Special Publication 4*, 1–89.